Spectral, thermal, kinetic, molecular modeling and eukaryotic DNA degradation studies for a new series of albendazole (HABZ) complexes

Nashwa M. El-Metwaly [a,*], Moamen S. Refat [b,c]

[a] Department of Chemistry, Faculty of Science, Mansoura University, Egypt
[b] Department of Chemistry, Faculty of Science, Port Said University, Port Said 42111, Egypt
[c] Department of Chemistry, Faculty of Science, Taif University, 888 Taif, Kingdom Saudi Arabia

ARTICLE INFO

ABSTRACT

This work represents the elaborated investigation for the ligational behavior of the albendazole ligand through its coordination with, Cu(II), Mn(II), Ni(II), Co(II) and Cr(III) ions. Elemental analysis, molar conductance, magnetic moment, spectral studies (IR, UV–Vis and ESR) and thermogravimetric analysis (TG and DTG) have been used to characterize the isolated complexes. A deliberate comparison for the IR spectra reveals that the ligand coordinated with all mentioned metal ions by the same manner as a neutral bidentate through carbonyl of ester moiety and NH groups. The proposed chelation form for such complexes is expected through out the preparation conditions in a relatively acidic medium. The powder XRD study reflects the amorphous nature for the investigated complexes except Mn(II). The conductivity measurements reflect the non-electrolytic feature for all complexes. In comparing with the constants for the magnetic measurements as well as the electronic spectral data, the octahedral structure was proposed strongly for Cr(III) and Ni(II), the tetrahedral for Co(II) and Mn(II) complexes but the square–pyramidal for the Cu(II) one. The thermogravimetric analysis confirms the presence or absence of water molecules by any type of attachments. Also, the kinetic parameters are estimated from DTG and TG curves. ESR spectrum data for Cu(II) solid complex confirms the square–pyramidal state is the most fitted one for the coordinated structure. The albendazole ligand and its complexes are biologically investigated against two bacteria as well as their effective effect on degradation of calf thymus DNA.

© 2010 Elsevier B.V. All rights reserved.

1. Introduction

Ligands containing heterocyclic aromatic units and their metal complexes have extensive applications in many types of technology [1,2]. Many heterocyclic compounds containing benzimidazoles, which are the nucleolus of albendazole are a subject of interest to medicinal chemistry because of the broad spectrum of their biological and pharmaceutical properties. Benzimidazole complexes have been investigated for their antifungal, antibacterial [3,4], antimicrobial [5,6], antiamoebic [7,8], antiparasitic [9] and antitumor activities [10,11]. Although the presence of many studies on benzimidazole complexes but the pharmacological or coordinative information about albendazole and some of its complexes is absent in the literature. A considerable number of metal complexes containing benzimidazole molecules is widely used in industry such Cu(II)-methylene-bis(N-methyl) benzimidazole is used in homopolimerization and co-polymerization of olefins and acry-

lates [12], Mn–binuclear complexes as a model to catalyses [13]. Recently, Ru–phenanthroline complexes with chelate ligands containing benzimidazoles and sulfur were reported to have a strong DNA binding and high anti cancer activity, being more potent than cisplatin against melanoma A375, and less toxic to normal cells [14]. Also, some biological studies have shown how analogous of ketone are effective as inhibitors of cell death [15]. Through out the previous work we abstract the importance of benzimidazole moiety, so the addition of other sites for the coordination (S and O) represents in albendazole ligand may reveal an expected distinguish behavior in coordination and application. In this study, we concern the synthesis, structural characterization and molecular modeling for the complexes with some metal ions in the first raw [Cu, Co, Ni, Cr and Mn]. Furthermore, the antimicrobial activity of the free ligand and its complexes against various pathogenic microorganisms was evaluated.

2. Experimental

2.1. Reagents

Albendazole used in our study was obtained from the Egyptian International Pharmaceutical Industrial Company (EIPICO). All

* Corresponding author. Current address: Department of Chemistry, Faculty of Education of Girls, Abha King Khalid University, Saudi Arabia.
Tel.: +966 0565370833.
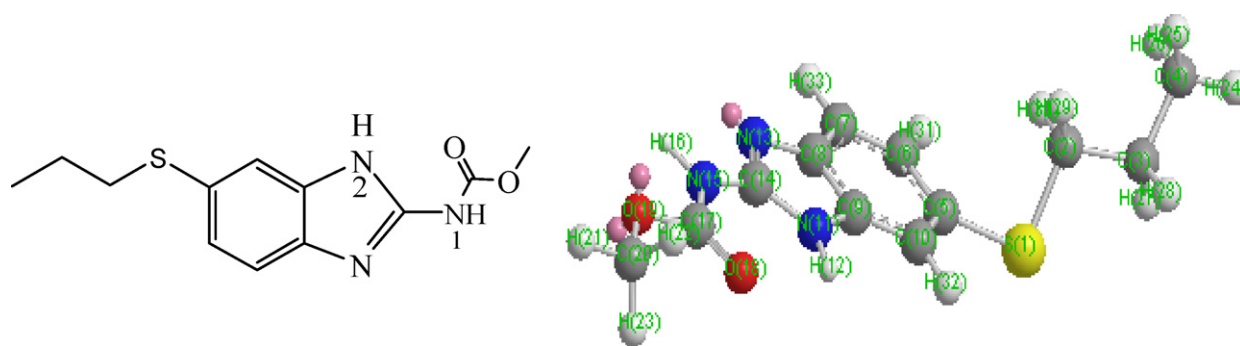*E-mail address:* n_elmetwaly00@yahoo.com (N.M. El-Metwaly).

Fig. 1. The structural and the modeling forms for the albendazole ligand.

Table 1
The molecular parameters of the ligand and its complexes.

The assignment of the theoretical parameters	The compound investigated	The theoretical data
Total energy	(1) [$C_{12}H_{15}N_3SO_2$]	−67,064.4562148 (kcal/mol)
Total energy		−106.874000637 (a.u.)
Binding energy		−3281.5352798 (kcal/mol)
Isolated atomic energy		−63,782.9209350 (kcal/mol)
Electronic energy		−428,514.5365246 (kcal/mol)
Core–core interaction		361,450.0803098 (kcal/mol)
Heat of formation		75.1927202 (kcal/mol)
Dipole moment		5.285 (Debyes)
Homo		−7.4858
Lumo		−1.8662
Total energy	(2) [Cu ($C_{12}H_{15}N_3SO_2$)$Cl_2 \cdot H_2O$]	−116,199.6007872 (kcal/mol)
Total energy		−185.175827994 (a.u.)
Binding energy		−3697.2963612 (kcal/mol)
Isolated atomic energy		−112,502.3044260 (kcal/mol)
Electronic energy		−756,611.6461754 (kcal/mol)
Core–core interaction		640,412.0453882 (kcal/mol)
Heat of formation		−90.2273612 (kcal/mol)
Dipole moment		10.058 (Debyes)
Homo		−8.1078
Lumo		−2.3574
Total energy	(5) [Co($C_{12}H_{15}N_3SO_2$)ClOH]$2H_2O$	−99,419.0368391 (kcal/mol)
Total energy		−158.434300465 (a.u.)
Binding energy		−3762.7467911 (kcal/mol)
Isolated atomic energy		−95,656.2900480 (kcal/mol)
Electronic energy		−644,522.8056797 (kcal/mol)
Core–core interaction		545,103.7688406 (kcal/mol)
Heat of formation		−215.0697911 (kcal/mol)
Dipole moment		7.341 (Debyes)
Homo		−8.3501
Lumo		−1.4854
Total energy	(6) [Cr($C_{12}H_{15}N_3SO_2$)Cl_3H_2O]$3H_2O$	−102,019.8059128 (kcal/mol)
Total energy		−162.578889288 (a.u.)
Binding energy		−3820.9944928 (kcal/mol)
Isolated atomic energy		−98,198.8114200 (kcal/mol)
Electronic energy		−750,132.7568776 (kcal/mol)
Core–core interaction		648,112.9509648 (kcal/mol)
Heat of formation		−170.6354928 (kcal/mol)
Dipole moment		9.559
Homo		−8.0914
Lumo		−1.6917

Table 2
Analytical and physical data for the Albendazole (HABZ) and its metal complexes.

| Compound empirical formula (M. Wt.)	Color	Elemental analysis (%) calcd. (found)				
		C	H	N	M	Cl
[$C_{12}H_{15}N_3SO_2$] (265.33)	White	54.3 (55.0)	5.7 (5.5)	15.8 (16.8)	–	–
[$CuCl_2 \cdot H_2O$($C_{12}H_{15}N_3SO_2$)] (417.80)	Olive green	34.5 (34.6)	4.1 (4.1)	10.1 (4.3)	15.2 (15.1)	16.9 (16.5)
[$MnCl_2$($C_{12}H_{15}N_3SO_2$)]$3H_2O$ (445.22)	Buff	32.4 (30.9)	4.7 (4.5)	9.4 (9.1)	12.3 (12.0)	15.9 (16.3)
[$NiCl \cdot OH(H_2O)_2$($C_{12}H_{15}N_3SO_2$)] (412.52)	Green	34.9 (34.2)	4.9 (4.3)	10.2 (10.6)	14.2 (14.6)	8.6 (9.0)
[$CoCl \cdot OH$($C_{12}H_{15}N_3SO_2$)]$2H_2O$ (412.76)	Green	34.9 (33.4)	12.9 (13.6)	3.2 (2.7)	24.1 (23.6)	8.6 (8.8)
[$CrCl_3 \cdot H_2O$ ($C_{12}H_{15}N_3SO_2$)]$3H_2O$ (495.76)	Green	26.1 (26.2)	4.7 (4.8)	8.5 (8.1)	10.5 (10.8)	21.4 (21.8)
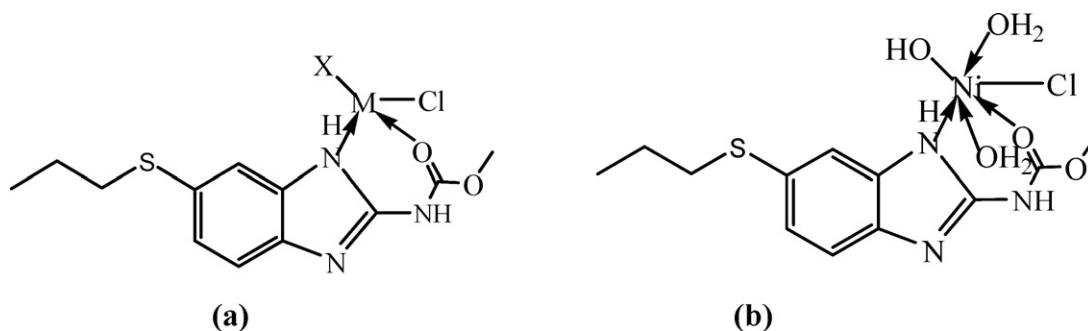
Fig. 2. (a) The structural form for two complexes (whereas: M = Co or Mn and X = OH or Cl, respectively), and (b) the structural form of Ni(II) complex.
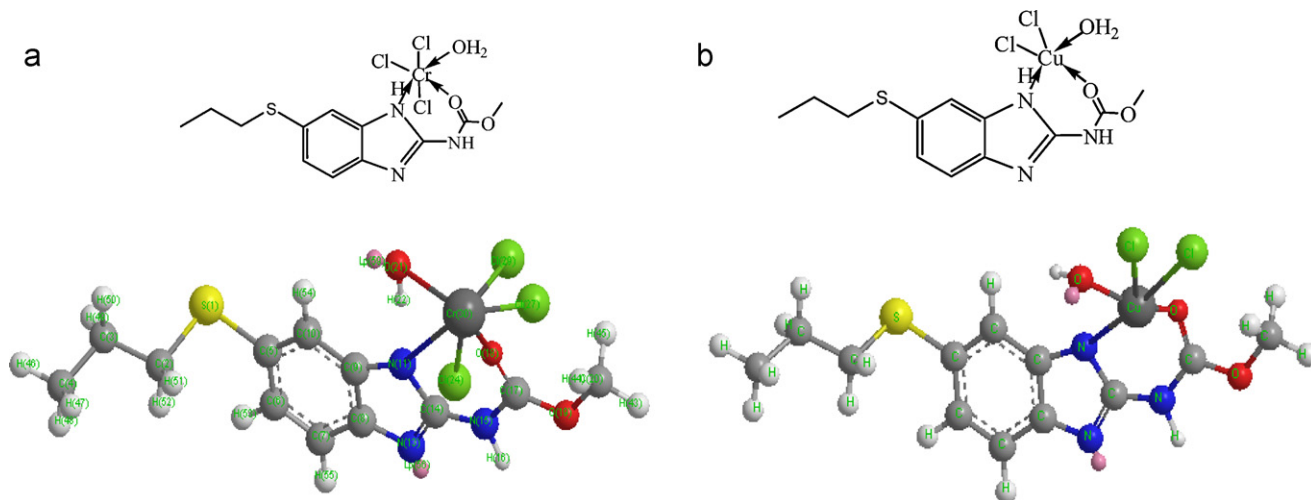

Fig. 3. (a and b) The structural form and the modeling structure of the Cr(III) and Cu(II) complexes, respectively.

Table 3
Assignments of the IR spectral bands (cm^{-1}) of HABZ and its metal complexes.

Compound	υ_{NH^1}	υ_{NH^2}	$\upsilon_{C=N}$	$\upsilon^I_{C=O}$	δ_{NH^1}	δ_{NH^2}	υ_{C-S}	υ_{M-N}	υ_{M-O}
(1) [C$_{12}$H$_{15}$N$_3$SO$_2$]	3149	2956	1629	1710	1525	1444	696	–	–
(2) [CuCl$_2$·H$_2$O (C$_{12}$H$_{15}$N$_3$SO$_2$)]	3300	2960	1631	1681	1589	1454	698	433	524
(3) [MnCl$_2$(C$_{12}$H$_{15}$N$_3$SO$_2$)]3H$_2$O	3299	2958	1627	1693	1530	1452	700	428	514
(4) [Ni·Cl·OH(H$_2$O)$_2$(C$_{12}$H$_{15}$N$_3$SO$_2$)]	3270	2958	1610	1689	1530	1454	701	439	518
(5) [Co·ClOH·(C$_{12}$H$_{15}$N$_3$SO$_2$)]2H$_2$O	3255	2966	1648	1710	1536	1463	701	470	526
(6) [Cr·Cl$_3$H$_2$O(C$_{12}$H$_{15}$N$_3$SO$_2$)]3H$_2$O	3270	2962	1635	1683	1550	1459	701	450	561

chemicals used for the study were of analytically reagent grade, commercially available from Fulka and used without previous purification as CoCl$_2$·6H$_2$O, CrCl$_3$·6H$_2$O, MnCl$_2$·4H$_2$O, NiCl$_2$·6H$_2$O and, CuCl$_2$·4H$_2$O compounds, which represents the metal ions in concern for the complexation.

2.2. Synthesis of the complexes

The complexes were prepared by heating 1:1 molar ratio for the ligand (0.2653 g, 1 mmol) with each metal chloride salt in methanolic medium in a water bath for 4–5 h under reflux. The precipitate

was filtered off washed with methanol and diethyl ether and finally dried in a vacuum desiccator. The [CoCl$_2$(H$_2$O)(HABZ)]3H$_2$O was synthesized [16] by dissolving 0.119 g (0.5 mmol) of Co(II) chloride in ethanol (10 ml) and added to hot ethyl acetate solution (10 ml) of HABZ (0.133 g, 0.5 mmol). The blue solution was refluxed for 4 h and the allowed to stand for 2 weeks. The resulting blue powder was filtered off washed with ethanol and dried in a vacuum. This complex is structurally similar with that isolated in our study, but the molecular formulas are partially different. This is accordance with the difference in synthesis procedures.

Table 4
Magnetic moments (BM) and electronic spectra bands (cm^{-1}) of the complexes.

Complex	μ_{eff} (BM)	d–d transition (cm^{-1})	Intraligand and charge transfer (cm^{-1})	Ligand field parameters		
				10 Dq (cm^{-1})	B (cm^{-1})	β
(2)	1.85	11,628	26,316; 36,496; 21,00	–	–	–
(3)	5.90	24,154	36,496; 34,014; 31,056; 26,042	–	–	–
(4)	2.83	14,662; 24,876	36,496; 34,014; 31,645; 30,120	11,781.1	279.6	0.27
(5)	4.45	14,837; 16,502	36,765; 34,482; 31,056	4750.7	570.8	0.59
(6)	3.72	16,286; 22,727	36,496; 34,722; 31,446	–	–	–

Table 5
Thermogravimetric data of the investigated complexes.

Complex	Steps	Temp. range (°C)	DTG peak (°C)	Decomposed assignments	Weight loss found (calcd.%)
(2)	1st	112.4–234.6	168.8	$-Cl_2 + H_2O$	20.99 (21.28)
	2nd	235.5–429.7	323.9	$-C_4H_{12}OS$	25.86 (25.90)
	3rd	528.6–787.0	681.3	$-C_7H_3N_3$	31.28 (30.91)
	Residue			$CuO + C$	21.87 (21.91)
(3)	1st	36.2–170.2	118.2	$-3H_2O$	12.52 (12.14)
	2nd	171.4–350.1	265.8	$-Cl_2$	15.21 (15.93)
	3rd	350.9–580.1	455.5	$-C_3H_8S$	16.98 (17.11)
	4th	580.1–790.2	680.1	$-C_7H_7N_3$	30.12 (29.91)
	Residue			$MnO_2 + 2C$	25.19 (24.92)
(4)	1st	154.1–268.3	204.8	$-OH + 2H_2O + 0.5\,Cl_2$	21.65 (21.45)
	2nd	269.9–488.6	347.9	$-C_3H_8S$	18.46 (18.87)
	3rd	490.1–675.4	575.7	$-C_9H_7N_3O$	42.03 (42.23)
	Residue			NiO	17.25 (18.11)
(5)	1st	30.8–148.4	71.5	$-2H_2O$	7.97 (8.73)
	2nd	149.2–250.7	191.1	$-0.5\,Cl_2 + H_2 + O_2$	16.92 (16.83)
	3rd	300.1–510.1	381.9	$-C_4H_{10}S$	21.13 (21.85)
	4th	511.6–785.1	672.8	$-C_7H_4N_3$	31.32 (31.53)
	Residue			$CoO + C$	22.66 (21.06)
(6)	1st	35.2–173.3	103.0	$-4H_2O$	14.55 (14.52)
	2nd	174.7–349.1	246.6	$-Cl_2$	14.47 (14.30)
	3rd	350.5–518.7	434.8	$-Cl_2 + CH_3OH$	13.84 (13.61)
	4th	520.3–779.4	636.0	$-C_{11}H_{11}N_3S$	43.72 (43.83)
	Residue			$Cr + 0.5\,O_2$	13.42 (13.71)

2.2.1. Antimicrobial activity

The ligand and its complexes were screened for their antimicrobial activity using the cup-diffusion technique [19] against *Bacillus thuringiensis* as gram positive and *Pseudomonas aeuroginosa* as gram negative bacteria. A 0.2 ml of the tested substance (10 µg/ml) was placed in specified cup made in the nutrient agar medium on which a culture of the tested bacteria has been spread to produce uniform growth. After 24 h incubation at 37 °C, the diameter of inhibition zone was measured as mm.

2.2.2. Genotoxicity

A solution of calf thymus DNA (2 mg) was dissolved in 1 ml of sterile distilled water to a final concentration of 2 g/l. Stock concentrations of the ligand, metal chloride salts and their complexes were prepared by dissolving 2 mg/ml in DMSO. An equal volume of each compound and DNA were mixed thoroughly and kept at room temperature for 2–3 h. The effects of the chemicals on the DNA were analyzed by agarose gel electrophoresis. A 2 µl of loading dye was added to 15 µl of the DNA–chemical mixture before being loaded into the wall of an agarose gel. The loaded DNA–chemical

Table 6
Kinetic parameters using the Coats–Redfern (CR) and Horowitz–Metzger (HM) operated for the Albendazole complexes.

| Complex	Step	Method	E (J mol^{-1})	A (S^{-1})	ΔS (J mol^{-1} K^{-1})	ΔH (J mol^{-1})	ΔG (J mol^{-1})	r
(2)	1st	CR	4.08×10^4	1.90×10^2	-2.05×10^2	3.71×10^4	1.27×10^5	0.9999
		HM	4.48×10^4	1.38×10^3	-1.88×10^2	4.11×10^4	1.24×10^5	0.9998
	2nd	CR	3.08×10^4	6.19×10^{-1}	-2.55×10^2	2.59×10^4	1.78×10^5	0.9988
		HM	3.46×10^4	3.13	-2.41×10^2	2.96×10^4	1.73×10^5	0.9992
	3rd	CR	1.02×10^5	9.24×10^2	-1.98×10^2	9.45×10^4	2.83×10^5	0.9999
		HM	1.23×10^5	2.17×10^4	-1.72×10^2	1.15×10^5	2.79×10^5	0.9997
(3)	1st	CR	2.43×10^5	2.39×10^{12}	-1.69×10^1	2.36×10^5	2.5×10^5	0.9999
		HM	2.78×10^5	3.52×10^{14}	-2.46×10^1	2.70×10^5	2.49×10^5	0.9993
(4)	1st	CR	5.36×10^4	2.57×10^3	-1.84×10^2	4.96×10^4	1.37×10^5	0.9992
		HM	6.62×10^4	1.55×10^5	-1.49×10^2	6.23×10^4	1.34×10^5	0.9994
	2nd	CR	8.78×10^4	5.81×10^4	-1.6×10^2	8.26×10^4	1.82×10^5	0.9994
		HM	9.37×10^4	5.68×10^5	-1.41×10^2	8.85×10^4	1.76×10^5	0.9997
	3rd	CR	1.62×10^5	3.85×10^7	-1.08×10^2	1.55×10^5	2.47×10^5	0.9999
		HM	1.7×10^5	2.22×10^8	-9.38×10^1	1.63×10^5	2.43×10^5	0.9999
(5)	1st	CR	9.57×10^3	3.53×10^{-2}	-2.74×10^2	6.71×10^3	1.01×10^5	0.9992
		HM	1.4×10^4	4.77×10^{-1}	-2.52×10^2	1.12×10^4	9.8×10^4	0.9996
	2nd	CR	8.35×10^4	1.88×10^7	-1.09×10^2	7.96×10^4	1.3×10^5	0.9999
		HM	8.87×10^4	1.18×10^8	-9.4×10^1	8.48×10^4	1.28×10^5	0.9999
	3rd	CR	8.73×10^4	2.95×10^4	-1.66×10^2	8.19×10^4	1.90×10^5	0.9999
		HM	9.55×10^4	2.81×10^5	-1.47×10^2	9.0×10^4	1.86×10^5	0.9998
	4th	CR	3.62×10^4	3.30×10^3	-1.87×10^2	2.84×10^4	2.05×10^5	0.9993
		HM	1.39×10^5	2.38×10^5	-1.52×10^2	1.32×10^5	2.75×10^5	0.9995
(6)	1st	CR	2.31×10^4	4.76	-2.34×10^2	2.0×10^4	1.08×10^5	0.9999
		HM	3.08×10^4	1.29×10^2	-2.06×10^2	2.77×10^4	1.05×10^5	0.9999
	2nd	CR	2.18×10^4	2.96×10^{-1}	-2.6×10^2	1.75×10^4	1.52×10^5	0.9996
		HM	3.13×10^4	4.96	-2.36×10^2	2.70×10^4	1.50×10^5	0.9995
	3rd	CR	3.91×10^4	1.19	-2.51×10^2	3.32×10^4	2.1×10^5	0.9992
		HM	5.01×10^4	1.51×10^1	-2.30×10^2	4.42×10^4	2.07×10^5	0.9993
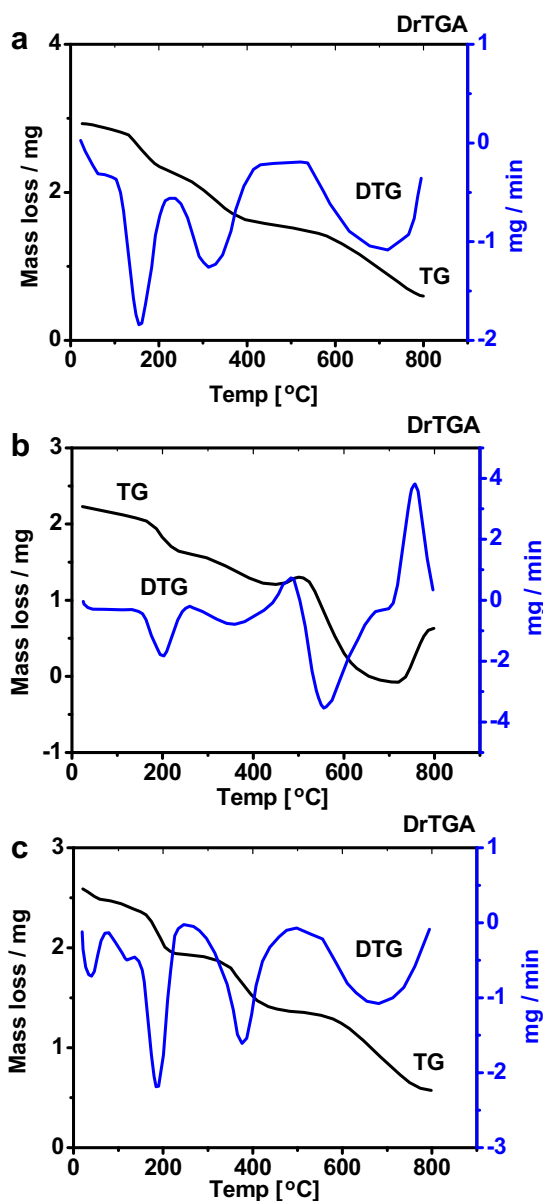
Fig. 4. (a) The TG and DTG curves of the Cu(II) complex thermogravimetric analysis and (b and c) of Ni(II) and Co(II) complexes, respectively.

mixtures were fractionated by electrophoresis, visualized by UV and photographed.

2.3. Molecular modeling

An attempt to obtain an acceptable insight about the molecular modeling structure of the ligand (Fig. 1) and some of its complexes was done. The geometry optimization and conformational analysis has been performed in Table 1 by the use of MM$^+$ [20] force-field as implemented in hyperchem 5.1 [21].

2.4. Physical measurements

Carbon, H and N were analyzed at the Microanalytical unit of Cairo University. Cu(II), Mn(II), Co(II), Ni(II) and Cr(III) were determined by complexometric titrations [17], but the conjugated chlorine was estimated gravimetrically [18] and the data reflect the high conformity. The molar conductivities of freshly prepared 1.0×10^{-3} mol/cm^3 DMSO solutions were measured for

the soluble complexes using Jenway 4010 conductivity meter. The X-ray diffraction patterns (XRD) were obtained on Pikagu diffractometer using Cu/Kα radiation. The infrared spectra, as KBr discs, were recorded on a Mattson 5000 FTIR Spectrophotometer (400–4000 cm^{-1}) at Mansoura University. The electronic and ^{1}H NMR (200 MHz) spectra were recorded on UV$_2$ Unicam UV/Vis, and a Varian Gemini Spectrophotometers, respectively in Mansoura and Cairo universities. The effective magnetic moments were evaluated at room temperature by applying $\mu_{eff} = 2.828\sqrt{X_M T}$, where X_M is the molar susceptibility corrected using Pascal's constants for the diamagnetism of all atoms in the ligand using a Johnson Matthey magnetic susceptibility balance. The thermal studies were carried out on a Shimadzu thermogravimetric analyzer at a heating rate of $10\,^\circ$C min^{-1} under nitrogen. ESR spectrum of solid Cu(II) complex was obtained on a Bruker EMX Spectrometer working in the X-band (9.78 GHz) with 100 kHz modulation frequency. The microwave power was set at 1 mW, and modulation amplitude was set at 4 Gauss. The low field signal was obtained after 4 scans with a 10-fold increase in the receiver gain. A powder spectrum was obtained in a 2 mm quartz capillary at room temperature. The biological study was carried out in Molecular Biology Center in Botany department in Mansoura University Egypt.

3. Results and discussion

The elemental analysis and some physical characteristics are summarized in Table 2. All the isolated complexes are stable in air, having high melting points, insoluble in H$_2$O and most organic solvents except DMSO and DMF. They are completely soluble except the Cr(III) and Ni(II) complexes. The molar conductivity measurements for $(1.0 \times 10^{-3}$ mol) in DMSO solvent are found with the range of non-conducting feature. This elucidates the proposal of analysis data for the presence of conjugated anion covalently attached with the central metal ion in the investigated complexes.

3.1. IR spectra of the complexes

Essential IR bands of the ligand and its complexes are tabulated in Table 3. In [CuCl$_2$·H$_2$O(HABZ)], [MnCl$_2$(HABZ)]3H$_2$O, [NiCl·OH·2H$_2$O(HABZ)], [CoCl·OH(HABZ)]2H$_2$O and [CrCl$_3$·H$_2$O(HABZ)]3H$_2$O complexes, the mode of coordination abstracted from a comparison of the spectra for the ligand and its complexes. This reflects that, the coordinated ligand is displaying the same manner in coordination with all metal ions as neutral bidentate through the oxygen of carbonyl ester group beside the NH one. The ligand behavior in the isolated complexes is satisfactory and acceptable due to the stereo structure of the arrangement of active donors with each others. This permits the bidentate attachment through the more electron dense groups. The obscure of the amide carbonyl deprotonation is supported by the preparation conditions represented in the relatively acidic medium of the precipitation. The mode of coordination proposed is confirmed through the molecular modeling of the most stable structure applying the hyperchem program. The IR spectrum of the ligand displays the υ(C=O) band at 1710, δNHs at 1525, 1444, υ(C–S) at 696 cm^{-1}, and υ(C=N) at 1629 cm^{-1}. The lower shift observed clearly in υ(C=O) band appeared at $\approx$1680 cm^{-1} in each complex spectrum supports its coordination in neutral state and represents the first side in coordination [22]. Also, more or less unshift observed for υ(C=N), υ(C–S) supports their siding out from complexation. The higher shift observed in υ and δ NH^1 bands supports their coordination after the intraligand hydrogen bonding disappearance. The appearance of new bands in all complexes spectra assigned to υM–O, υM–N and υM–Cl supports the proposed coordination sites surrounds the central atoms. The water

of hydration molecules proposed in the Mn(II), Co(II) and Cr(III) complexes caused a little broad suffered in the higher field area (3400–3480 cm^{-1}), but the coordinated water displays bands at ≈720, ≈600, ≈630 cm^{-1} assigned for δr, δw and δt H_2O molecules. It should be mentioned here, that these assignments for both the bond stretches and angular deformation of the coordinated water molecules fall in the frequency regions reported for other related complexes [22].

3.2. Spectral and magnetic studies

The magnetic measurements for the isolated complexes and their significant electronic spectral bands are presented in Table 4. The spectra for all complexes under investigation were carried out in DMF solution. The spectrum of a highly diluted solution of the ligand reveals bands in UV region (34,246 and 33,112 cm^{-1}) assigned for intraligand transitions ($\pi \rightarrow \pi^*$ and $n \rightarrow \pi^*$, respectively). The magnetic moment of [MnCl$_2$·(HABZ)]3H$_2$O complex is 5.9 BM, as a high spin complex for d^5 configuration, near the spin only magnetic moment value (5.8 BM). The electronic transition band at 24,154 is clearly indicating the tetrahedral coordination around manganese(II) for $A_1^6 \rightarrow A_1^4(g)$ transition [23]. The electronic spectrum of green [CoCl·OH(HABZ)]2H$_2$O complex (Fig. 2) exhibits one characteristic band at 14,837 cm^{-1} attributed to $^4A_2 \rightarrow ^4T_1(P)$ transition referring to tetrahedral structure. The shoulder at 16,502 cm^{-1} may be due to the spin coupling [24] also the magnetic moment value (4.45 BM) within the range reported for such structures. The green color is considered the additional evidence for the tetrahedral postulation. The ligand field parameters (B, β and 10 Dq) are calculated, according to equations reported for tetrahedral Co(II) complexes:

$$\mu_{eff} = 3.87 \left(\frac{1 - 4\lambda}{10\,Dq} \right) \quad \lambda = -178\,cm^{-1}$$

$$B = \frac{4(\upsilon_3 - 15\,Dq)^2 - 10\,Dq^2}{60(\upsilon_3 - 15\,Dq) - 18\Delta}$$

$$\upsilon_1 = 10\;Dq$$

The calculated values (570.78, 0.588 and 4750.75) are found in the range reported for the suggested structure. The β value (0.59) indicates more covalent character for Co(II)–ligand bonds. The transition for $^4A_2 \rightarrow ^4T_2(\upsilon_1)$ is calculated to be 4750.7 cm^{-1}. The magnetic moment of [NiCl·OH·2H$_2$O(HABZ)] complex (Fig. 2b) is found to be 2.83 BM within the range of six-coordinate Ni(II) complex at room temperature and corresponding to the two unpaired electrons. The spectral bands for the d–d transition appeared at 14,662 and 24,876 cm^{-1} attributed to $^3A_2g(F) \rightarrow ^3T_1g(F)(\upsilon_2)$ and $^3A_2g \rightarrow ^3T_1g(P)(\upsilon_3)$, transitions, respectively in an octahedral geometry. The Ni(II) complex reflects the trend of increasing the size of the ligand the lower shift in the energy of the maxima d–d bands, presumably due to weakening of the coordinate bond with increased bulkiness of the ligand [25]. The spectrochemical parameters 10 Dq, B and β are calculated applying the following equations:

$$\Delta = 10\,Dq = \frac{(\upsilon_2 + \upsilon_3)}{3} - 5B$$

$$340B^2 - 28\left(\frac{\upsilon_2 - \upsilon_3}{3}\right)B + \left(\frac{\upsilon_2 - \upsilon_3}{3}\right)^2 - (\upsilon_3 - \upsilon_2)^2 = 0$$

for Ni(II) octahedral systems. The values are found to be 11,781.1, 279.6 and 0.27. The 10Dq value (11,781.1 cm^{-1}) is found within the normal range for $^3A_2g \rightarrow ^3T_2g(F)(\upsilon_1)$ transition, the B value is considered to be ≈27% indicating highly covalent character

for the interaction between Ni(II) and ligand sites [26] of coordination. The lower B value is reflecting the highly changeable in nuclear charge for the cation. The parameter β is highly low, this supporting the covalent character for the coordination with N and O atoms in comparing with that reported for NiN$_6$ and NiO$_6$. The [CrCl$_3$(H$_2$O)(HABZ)]3H$_2$O complex (Fig. 3a) exhibit three bands at 31,446, 22,727 and 16,286 assigned to $^4A_2g(F) \rightarrow ^4T_1g(P)$, $^4A_2g(F) \rightarrow ^4T_1g(F)$ and $^4A_2g(F) \rightarrow ^4T_2g(P)$ transitions, respectively. The magnetic moment (3.72 BM) is well within the range for three unpaired electrons. The electronic spectral bands beside the magnetic moment support strongly the octahedral for the geometry around the Cr ion. The electronic spectrum of [CuCl$_2$·H$_2$O(HABZ)] olive green complex (Fig. 3b) does not reveal any absorption bands at 20,000 cm^{-1} for S → Cu charge transfer transition [27], which supports its absence from coordination for the square-based pyramid geometry in a close to C$_{4v}$ group. (For interpretation of the references to color in text, the reader is referred to the web version of the article.) There are three spin allowed transitions as $^2B_1 \rightarrow ^2A_1$, $^2B_1 \rightarrow ^2B_2$ and $^2B_1 \rightarrow ^2E_1$ usually very difficult to resolve them into separate bands due to the very low energy difference between these bands, so appeared at 11,628 cm^{-1}. Band at ≈21,000 cm^{-1} is attributed to O → Cu charge transfer transition. The intense band at ≈26,316 cm^{-1} is attributed to N → Cu charge transfer transition. The magnetic moment of the complex [1.85 BM] within the normal range reported for d^1 systems and also, reflects the absence of any metal–metal interaction for mononuclear complex. All the bands at higher region ≈36,000–34,000 cm^{-1} assigned to intraligand $\pi \rightarrow \pi^*$ and $n \rightarrow \pi^*$ transitions, suffered marginal shift from that of their corresponding free ligand. However, some charge transfer bands may also be present in this region for the complexes [26].

3.3. Thermal analysis

The decomposition stages, temperature ranges, proposed decomposition products as well as the calculated and found weight loss percentages of the complexes are presented in Table 5. In most investigated complexes, the first decomposition stage is attributed to the removal of hydrated water molecules. The kinetic parameters for the thermal behavior of the complexes are calculated in Table 6. In [CuCl$_2$·H$_2$O(HABZ)] complex, the TG and DTG curves show three decomposition stages (Fig. 4a) started at 112.4 °C and ended at 787.04 °C. The complex reveals a relative thermal stability up to 112 °C and followed by a sudden decomposition by a weight loss 20.99 (calcd.21.28%) corresponding to the elimination of coordinated H$_2$O and Cl$_2$ molecules. The second exothermic decomposition stage started at 235.5 °C corresponding to the removal of C$_4$H$_{12}$OS as a terminal organic moiety by 25.86 (calcd.25.90%) weight loss. The final degradation stage started at 528.6 °C is translated to the removal of another organic moiety (C$_7$H$_3$N$_3$) by 31.28 (calcd.30.91) weight loss lefts CuO at ≈800 vC as a residual polluted with carbon atom. The gradual degradation stages for [MnCl$_2$(HABZ)]3H$_2$O complex started at 36.17 °C and attributed to the dehydration for 3H$_2$O by 12.52 (calcd.12.14%) weight loss. The removal of Cl$_2$ in the following decomposition stage started at 171.42 °C by 15.21 (calcd.15.93%) weight loss. The removal of major organic part in coordinator [C$_3$H$_8$S + C$_7$H$_7$N$_3$] in third and fourth steps started as 350.91 and 580.12 °C by 16.98 (calcd.17.11%) and 30.12 (calcd.29.92%) weight loss, respectively. The final residue is MnO$_2$ polluted with carbon atoms. The gradual degradation stages representing in TG and DTG curves for [NiCl·OH·2H$_2$O (HABZ)] complex (Fig. 4b) started at 154.1 °C for the first degradation stage after legal thermal stability is attributed to the removal of 2H$_2$O + 0.5Cl$_2$ + OH, by 21.65 (calcd.21.45%) weight loss. The removal of C$_3$H$_8$S + C$_9$H$_7$N$_3$O as a whole organic moieties in the two following steps started at 269.92 and 490.15 °C by 18.46 (calcd.18.87%) and 42.03 (calcd.42.23%) weight loss. The
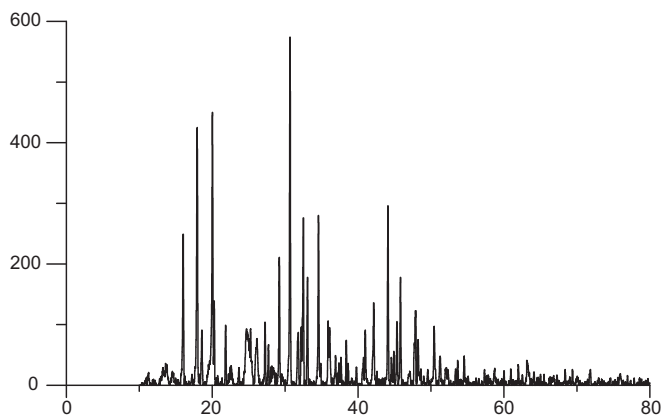
Fig. 5. The XRD diagram of the Mn(II) albendazole complex.

residual part is NiO by 17.25 (calcd.18.11%) weight. The gradual degradation stages representing in TG and DTG curves for [CoCl·OH (HABZ)]2H$_2$O complex (Fig. 4c) started with sudden decomposition at low temperature 30.85 °C referring to the expel of two hydrated H$_2$O molecules by 7.97 (calcd.8.73%) weight loss. The second decomposition step started at 149.17 °C attributed to the removal of H$_2$ + O$_2$ + 0.5Cl$_2$ by 16.92 (calcd.16.83%) weight loss. The final steps reveal the removal of organic part (C$_4$H$_{10}$S and C$_7$H$_4$N$_3$) by 21.13 (calcd.21.85%) and 31.32 (calcd.31.53%) weight loss. The residual part is CoO contaminated with carbon atom. The gradual degradation stages representing in TG and DTG curves for [CrCl$_3$(H$_2$O)(HABZ)]3H$_2$O complex started with sudden decomposition at 35.17 °C reflecting the thermal instability referring to the hydrated water molecules expelled in the first step beside the coordinated one by 14.55 (calcd.14.52%) weight loss. The removal of Cl$_2$ molecule by 14.47 (calcd.14.30%) in the second step started is carried out at 174.7 °C. The removal of 0.5Cl$_2$ + CH$_3$OH molecules at the third step started at 350.5 °C by 13.84 (calcd.13.61%) weight loss. The C$_{11}$H$_{11}$N$_3$S organic moiety is expelled completely at 779.4 °C as the final part by 43.72 (calcd.43.83%) weight losses. The residual part represents in Cr + 0.5O$_2$ by 13.42 (calcd.13.71%) weights.

3.4. Kinetic studies

In order to assess the effect of the metal ion on the thermal behavior of the complexes, the order n, and the heat of activation E of the various decomposition stages were determined from the TG and DTG. Several equations [28–35] have been proposed as means of analyzing a TG curves and obtaining values for kinetic parameters. Many authors [28–31] have discussed the advantages of this method over the conventional isothermal method. The rate of the decomposition process can be described as the product of two separate functions of temperature and conversion [29], using:

$$\frac{d\alpha}{dt} = k(T)f(\alpha) \tag{1}$$

where α is the fraction decomposed at time t, $k(T)$ is the temperature dependant function and $f(\alpha)$ is the conversion function dependent on the mechanism of decomposition. The temperature dependent function $k(T)$ is of Arrhenius type and can be considered as the rate constant k,

$$K = Ae^{-E*/RT} \tag{2}$$

where R is the gas constant in (J mol^{-1} k^{-1}) substituting Eq. (2) into Eq. (1) we get this equation:

$$\frac{d\alpha}{dT} = \left(\frac{A}{\varphi e^{-E*/RT}}f(\alpha)\right) \tag{3}$$

where φ is the linear heating rate dT/dt. From the integration and approximation, this equation can be obtained in the following form:

$$\ln g(\alpha) = \frac{-E*}{RT} + \ln\left[\frac{AR}{\varphi E*}\right]$$

where $g(\alpha)$ is a function of α dependant on the mechanism of the reaction. The integral on the right hand side is known as temperature integral and has no closed for solution. So, several techniques have been used for the evaluation of temperature integral. Most commonly used methods for this purpose are the differential method of Freeman and Carroll [28] integral methods of Coat and Redfern [30], the approximation method of Horowitz and Metzger [35]. The kinetic parameters for the albendazole complexes are evaluated using the following methods and the results are in good agreement (Table 6) with each other. The used methods are discussed briefly:

3.4.1. Coats–Redfern equation

The equation is a typical integral method, represented as:

$$\int_0^\alpha \frac{d\alpha}{(1-\alpha)^n} = \frac{A}{\varphi}\int_{T_1}^{T_2} \exp\left(\frac{-E*}{RT}\right) dt$$

For convenience of integration the lower limit T_1 is usually taken as zero. This equation on integration gives:

$$\ln\left[\frac{-\ln(1-\alpha)}{T^2}\right] = \ln\left(\frac{AR}{\varphi E*}\right) - \frac{E*}{RT}$$
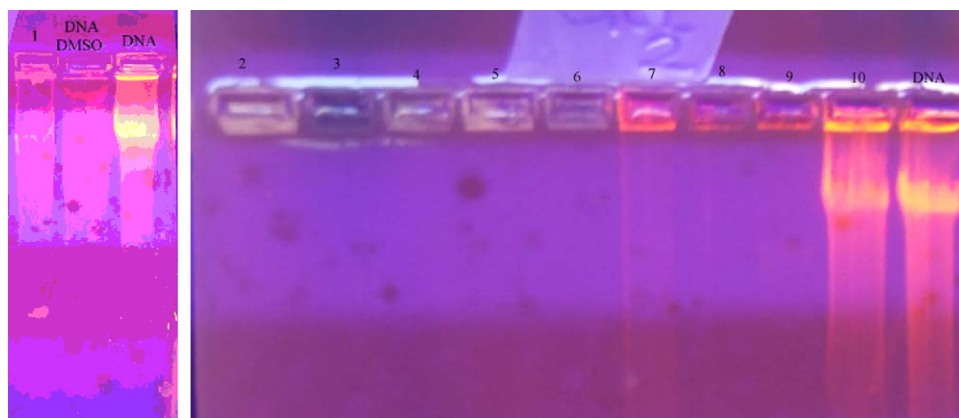

Fig. 6. Electrophoretic mobility of Calf thymus DNA treated with HABZ (lane 1), Cr complex (lane 2), Co complex (lane 3), Cu complex (lane 4), Mn complex (lane 5), Ni complex (lane 6), lanes from 7 to 10 represents the chloride salts of each metal ion used except Cr, respectively, the final represent control calf thymus DNA sample.

Table 7
ESR data of Cu(II) complex at room temperature.

Complex	$g_{//}$	$g_\perp$	g_{av}	$A_{//} \times 10^{-4}$ (cm^{-1})	G	α^2	β^2
(2)	2.093	2.03	2.062	160	3.1	0.59	0.27

A plot of $\ln[-\ln(1-\alpha)/T^2]$ (LHS) against $1/T$ was drawn. E^* is the energy of activation in $J\,mol^{-1}$ and calculated from the slop and A is (S^{-1}) from the intercept value. The entropy of activation ΔS^* in $(J\,K^{-1}\,mol^{-1})$ was calculated by using the equation:

$$\Delta S_* = R \ln \left(\frac{Ah}{K_B T_s} \right) \tag{4}$$

where k_B is the Boltzmann constant, h is Plank's constant and T_s is the DTG peak temperature [36].

3.4.2. Horowitz–Metzger equation
The authors derived the relation:

$$\ln[-\ln(1-\alpha)] = \frac{E}{RT_m}\Theta \tag{5}$$

where α is the fraction of the sample decomposed at time t and $\Theta = T - T_m$.

A plot of $\ln[-\ln(1-\alpha)]$ against Θ, was found to be linear, from the slope of which E, was calculated and Z can be deduced from the relation:

$$Z = \frac{E\varphi}{RT_m^2} \exp \left(\frac{E}{RT_m} \right) \tag{6}$$

where φ is the linear heating rate, the order of reaction, n, can be calculated from the relation:

$$n = 33.64758 - 182.295\alpha_m + 435.9073\alpha_m^2 - 551.157\alpha_m^3$$
$$+ 357.3703\alpha_m^4 - 93.4828\alpha_m^5 \tag{7}$$

where α_m is the fraction of the substance decomposed at T_m.

The entropy of activation, ΔS^*, was calculated from Eq. (4). The enthalpy of activation ΔH^*, and Gibbs free energy, ΔG^*, were calculated from; $\Delta H^* = E^* - RT$ and $\Delta G^* = \Delta H^* - T\Delta S^*$, respectively. The data tabulated reveals the following observations: (i) the activation energy E, increases somewhat through the degradation steps revealing the high stability of the remaining part suggesting a high stability of complexes characterized by their covalence, (ii) the negative ΔS^* values, indicates the activated fragment has ordered structures, (iii) the positive ΔH^* reflects the endothermic decomposition process, (iv) the positive ΔG^* singe reveals that the free energy of the final residue is higher than that of the initial compound, and the decomposition stages are non-spontaneous. This results from increasing $T\Delta S^*$ clearly from one step to another which override the values of ΔH^* reflecting that the rate of removal of the subsequent species will be lower than that of the precedent one [36].

3.5. ESR spectrum

The spin Hamiltonian parameters and the G value of solid state Cu(II) complex are calculated (Table 7). Its ESR spectrum displayed axially symmetric g tensor parameters with $g_{11} > g_\perp > 2.0023$ indicating that the $d_{x^2-y^2}$ orbital as a ground state [37]. In axial symmetry the g-values are related to the G-factor by the expression, $G = (g_{11} - 2)/(g_\perp - 2) = 4$, which measures the exchange interaction between copper centers in the solid. According to Hathaway [38], if the value of G is greater than 4, the exchange interaction between copper(II) centers in the solid state is negligible, whereas when it is less than 4, a considerable exchange interaction exists in the solid complex. The G value is less than 4 (3.1), this supports the little presence of exchange coupling between copper(II) centers in the solid

Table 8
The values of zone inhibition of bacteria for the ligand and its metal complexes.

Compound	Zone of inhibition (mm)	
	Bacillus thuringiensis Gram (+) bacteria	Pseudomonas aeuroginosa Gram (−) bacteria
(1) HABZ	0	0
(2)	16	0
(3)	0	0
(4)	20	0
(5)	16	0
(6)	16	0

state [39]. This hyperfine interaction observed for the complex is attributed to the interaction with nitrogen and oxygen nuclei adjacent to copper ion. Kivelson and Neiman [40] have reported the g_{11} value <2.3 for covalent character of the metal–ligand bond and >2.3 for ionic character. Applying this criterion the covalent character of the metal–ligand bond in the complex under study can be predicated. The trigonal bipyramidal and square–pyramidal have a ground state configuration $^2B_1$ (unpaired electron in $d_{x^2-y^2}$ orbital) and $^2A_1$ (unpaired electron in d_{z^2} orbital), respectively. Molecular orbital coefficients, α^2 (A measure of the covalence of the in-plane σ-bonding between a copper 3d orbital and the ligand orbital) and β^2 (covalent in-plane π-bonding), were calculated by using the following equations [40–44], where $\alpha^2 = 1$ indicates complete ionic character, whereas $\alpha^2 = 0.5$ denotes 100% covalent bonding, with the assumption of negligibly small values of the overlap integral.

$$\alpha^2 = ((A_{//}/0.036) + (g_{//} - 2.0023) + 3/7(g_\perp - 2.0023) + 0.04$$

$$\beta^2 = (g_{//} - 2.0023)E/ - 8\lambda\alpha^2,$$

where $\lambda = -828\,cm^{-1}$ for the free copper ion and E is the electronic transition energy. From Table 7, the α^2 and β^2 values indicate that the in-plane σ-bonding and the in-plane π-bonding are highly covalent. The lower value of β^2 compared to α^2 indicates that the in-plane π-bonding is more covalent than the in-plane σ-bonding. The α^2 value for copper(II) complex indicates a considerable covalency in the bonding between the Cu(II) ion and the ligand.

3.6. Molecular modeling of the ligand and some of its complexes

The atomic numbering scheme and the theoretical geometry structures for the ligand and some of its metal complexes are calculated. The molecular parameters: total energy, binding energy, isolated atomic energy, electronic energy, heat of formation, dipole moment, HOMO and LUMO were calculated and represented in Table 1. A comparison between the bond length of the ligand and its complexes is illustrated. The length of C=O$_{ligand}$ and C–N bonds are found high in complexes than that in the free ligand indicating their participation in complexation. However, the length of C=N bond does not change.

3.7. Ray powder diffraction of some complexes

X-ray powder diffraction pattern in the $10° < 2\theta < 70°$ of the Cu(II), Cr(III) and Mn(II) complexes were carried in order to give an insight about the lattice dynamics of the compounds. The X-ray powder diffraction obtained reflects a shadow on the fact that each solid represents a definite compound of a definite structure which is not contaminated with starting materials. This identification of the complexes was done by the known method [45]. Such facts suggest that the Cu(II) and Cr(III) complexes are amorphous but Mn(II) is nanocrystalline (Fig. 5).

3.8. Biological activity

3.8.1. Eukaryotic DNA degradation effect

The DNA degradation behavior under the effect of the ligand, metal salts and their complexes is examined. A deliberate comparison reflects the completely difference in the results obtained after mixing the calf thymus DNA with the ligand and with each complex. The results shown in the photos (Fig. 6) the ligand and DMSO did not degrade the DNA and the DNA migration was close to the top of the gel. Whereas, all the complexes degraded the DNA almost completely in comparing with their original chloride salts. This behavior is illustrated referring to the direct contact of the complexes with the DNA which able to degrade it.

3.8.2. Antimicrobial activity

The ligand and its complexes were tested against Gram-positive (*Bacillus thuringiensis*) and Gram-negative (*Pseudomonas aeuroginosa*) bacteria for their antibacterial activities (Table 8) using the disc diffusion sensitivity testing method. The Ni(II), Cu(II), Co(II) and Cr(III) complexes inhibited the growth of G +ve Bt bacterium, whereas all the complexes were non-effective against the G −ve bacterium. The best antibacterial complex is the Ni(II) one which showed moderate antibacterial activity, while Cr(III), Co(II) and Cu(II) complexes showed weak activity against Gram-positive bacterium. The negative results can be attributed either to the in ability of the complexes to diffuse into the Gram-negative or the Gram-positive bacterium and hence unable to interfere with its biological activity or they can diffuse and inactivated by unknown cellular mechanism by the bacterium. The positive results suggested the diffusion of the complexes inside the Bt cells and killed bacteria as indicated by the zones of inhibition diameter.

References

[1] D.A. Horton, G.T. Bourne, M.L. Smythe, Chem. Rev. 103 (2003) 893.
[2] H. Kucukbay, R. Durmaz, E. Orhan, S. Gunal, II Farmaco 58 (2003) 431.
[3] V.K. Limesova, J. Koci, K. Waisser, J. Kaustova, II Farmaco 57 (2002) 259.
[4] Y. He, B. Wu, J. Yang, D. Robinson, L. Risen, R. Ranken, L. Blyn, S. Sheng, E.E. Swayze, Bioorg. Med. Chem. Lett. 13 (2003) 3253.
[5] G. Ayhan, N. Altanlar, II Farmaco 58 (2003) 1345.
[6] N.S. Pawar, D.S. Dalal, S.R. Shimpi, P.P. Mahulikar, Eur. J. Pharm. Sci. 21 (2004) 115.
[7] N.B. Shailendra, M.T.G. Garza, D.E.C. Vega, J. Castrogarza, K. saleem, F. Naqui, M.R. Maurya, A. Azam, Med. Chem. Lett. 12 (2002) 869.
[8] S. Ozden, D. Atabey, S. Yildiz, H. Goker, Bioorg. Med. Chem. 13 (2005) 1587.
[9] G. Navarrete-Vazquez, R. Cedillo, A. Hernandez-Campos, J. Yepez, F. Hernndez-Luis, J. Valldez, R. Morales, R. Cortes, M. Hernandez, Bioorg. Med. Chem. Lett. 11 (2001) 187.
[10] A.A. Spasov, I.N. Yozhitsa, L.I. Bugavea, V.A. Anisimova, J. Pharm. Chem. 33 (1999) 232.
[11] T.A. Kabanos, A.D. Kersmidas, D. Mentzafos, U. Russo, A. Terzis, J.M. Tsangaris, J. Chem. Soc. Dalton Trans. (1992) 2729.
[12] R.T. Stibrany, D.N. Schulz, S. Kacker, A.O. Patil, L.S. Baugh, S.P. Rucker, S. Zushma, E. Berluche, J.A. Sissano, Macromolecules 36 (2003) 8584.
[13] A.E.M. Boelrijk, S.V. Khangulov, G.C. Dismukes, Inorg. Chem. 39 (2000) 3009.
[14] V. Rajendiran, M. Murali, E. Suresh, S. Sinha, K. Somasundaram, M. Palaniandavar, Dalton Trans. (2008) 148.
[15] C.M. Bitler, P.L. Wood, D.T. Anstine, A. Meyer-Franke, Q. Zhao, M.A. Khan, US Patent 6,541,486 (2003).
[16] H.L. Sandoval, M.E.L. Lemos, R.G. Velasco, I.P. Melendez, P.G. Macias, I.G. Mora, N.B. Behrens, J. Inorg. Biochem. 102 (2008) 1267–1276.
[17] C.N. Reilley, R.W. Schmid, F.S. Sadek, J. Chem. Edu. 36 (1959) 555.
[18] A.I. Vogel, Text Book of quantitative Inorganic Analysis, Long-man, London, 1986, p. 505.
[19] S.D. Dhmwad, K.B. Gudasi, T.R. Goudar, Ind. J. Chem. 33 (A) (1994) 320.
[20] N.L. Allinger, J. Am. Chem. Soc. 99 (1977) 8127.
[21] Hyper chem, Version 7.51, Hyper cube, Inc.
[22] K. Nakamoto, P.J. McCarthy, Spectroscopy and Structure of Metal Chelate Compounds, John Wiley, New York, 1968, p. 268.
[23] C.K. Jorgensen, Chim. Inorg, Acta Rev. 2 (1962) 65.
[24] P.K. Panda, S.B. Mishra, B.K. Mohapatka, J. Inorg. Nucl. Chem. 42 (1980) 497.
[25] L. Latheef, R. Maliyeckal, P. Kurup, Polyhedron 27 (2008) 35–43.
[26] A.B.P. Lever, Inorganic Electronic Spectroscopy, Elsevier, Amsterdam, 1986.
[27] E. franco, E. Lopez–Torres, M.A. Mendiola, M.T. Sevilla, Polyhedron 19 (2000) 441.
[28] E.S. Freeman, B. Carroll, J. Phys. Chem. 62 (1958) 394.
[29] J. Sestak, V. Satava, W.W. Wendlandt, Thermochim. Acta 7 (1973) 333.
[30] A.W. Coats, J.P. Redfern, Nature 201 (1964) 68.
[31] T. Ozawa, Bull. Chem. Soc. Jpn. 38 (1965) 1881.
[32] W.W. Wendlandt, Thermal Methods of Analysis, Wiley, New York, 1974.
[33] J.H.F. Flynn, L.A. Wall, J. Res. Natl. Bur. Stand. A 70 (1996) 487.
[34] P. Kofstad, Nature 179 (1957) 1362.
[35] H.W. Horowitz, G. MJetzger, Anal. Chem. 35 (1963) 1464.
[36] S.S. Kandil, G.B. El-Hefnawy, E.A. Baker, Thermochim. Acta 414 (2004) 105.
[37] H.I. Park, L.J. Ming, J. Inorg. Biochem. 27 (1998) 57–62.
[38] (a) B.J. Hathaway, D.E. Billing, Coord. Chem. Rev. 5 (1970) 143;
(b) B.J. Hathaway, Struct. Bond. (Berl.) 57 (1984) 55.
[39] H. Montgomery, E.C. Lingefetter, Acta Cryst. 20 (1966) 728.
[40] D. Kivelson, R. Neiman, J. Chem. Phys. 35 (1961) 149.
[41] R.K. Ray, G.B. Kauffman, Inorg. Chem. Acta 174 (1990) 257–262.
[42] K. Jayasubramanian, S.A. Samath, S. Thambidurai, R. Murugesan, S.K. Ramalingam, Trans. Met. Chem. 20 (1995) 76.
[43] V.S.X. Anthonisamy, R. Murugesan, Chem. Phys. Lett. 287 (1998) 353.
[44] V.S.X. Anthonisamy, R. Anantharam, R. Murugesan, Spectrochim. Acta. A55 135 (1999).
[45] B.D. Cullity, Elements of X-ray Diffraction, second ed., Addison-Wesley Inc., 1993.